Rapid Communications

Engineering of heralded narrowband color-entangled states

A. Zavatta*
Istituto Nazionale di Ottica (CNR-INO) Largo E. Fermi, 6, 50125 Firenze, Italy;
European Laboratory for Nonlinear Spectroscopy, Via N. Carrara 1, 50019 Sesto Fiorentino, Italy;
and Dipartimento di Fisica ed Astronomia, Università degli Studi di Firenze, 50019 Sesto Fiorentino, Italy

M. Artoni
European Laboratory for Nonlinear Spectroscopy, Via N. Carrara 1, 50019 Sesto Fiorentino, Italy;
Istituto Nazionale di Ottica (CNR-INO) Via Branze 45, 25123 Brescia, Italy;
and Department of Information Engineering, Brescia University, 25123 Brescia, Italy

G. La Rocca
Scuola Normale Superiore and CNISM, 56126 Pisa, Italy

(Received 27 April 2018; published 19 March 2019)

The efficient generation of entanglement is an essential requirement for quantum communications; however, long distances can only be achieved by utilizing entangled states that can be efficiently mapped into matter. Hence, sources generating states with bandwidths naturally compatible with the linewidths of atomic transitions are crucial. We harness the indistinguishability between two spontaneous four-wave mixing processes to achieve the heralded generation of single-photon frequency-bin entangled states. State manipulation admits entanglement and generation probability optimizations yet with negligible absorption. The scheme could also be adapted to photonic and solid interfaces.

DOI: 10.1103/PhysRevA.99.031802

Introduction. Quantum states of light are crucial for quantum communications as well as for all emerging quantum technologies. The propagation of quantum states through optical channels is, however, dramatically affected by losses, making quantum networks a hard task to accomplish. In spite of this, the seminal paper of Duan *et al.* [1] proposed long-distance quantum communications through the entanglement of distant atomic ensembles. Since then, growing attention has been devoted towards the development of narrowband sources of quantum states of light to efficiently map light into atoms. Recently, several generation schemes based on spontaneous four-wave mixing and Raman processes in atomic ensembles have been proposed and demonstrated, such as, e.g., entangled photon pairs generated in trapped cold atoms [2–5], and in hot atoms vapor cells [6]. In such schemes, the quantum states can be generated with bandwidths naturally compatible with the atomic transitions, allowing a more efficient mapping of light into matter. Unfortunately, such processes are probabilistic and the generation happens at random times with very low probabilities. In order to circumvent this limitation, so-called heralded schemes, where desired output states are announced by ancillary photons, are required to allow both further processing into quantum communication networks and quantum state characterization [7].

Within this context, it is convenient to exploit the multilevel structure of resonant media such as atoms or atomlike systems [8–10], in order to engineer the generation of quantum states in a frequency multimode scenario [11,12]. In this Rapid Communication, we propose a scheme for the heralded generation of single-photon color-entangled states, i.e., states where a single-photon excitation is simultaneously shared by two distinct frequency modes of light, exploiting indistinguishability between four-wave mixing processes. We show that narrowband color-entangled states can be engineered and efficiently generated only if some specific conditions between detunings and Rabi frequencies of pump and coupling fields are met. Propagation [13] and mapping [14] onto a quantum memory of color-entangled states through a specific atomic interface has recently been studied, hence the present Rapid Communication represents an additional building block toward the realization of a quantum network, in which color entanglement is generated, manipulated, and stored.

The underlying physical mechanism hinges on a four-photon spontaneous four-wave mixing process in a three-level third-order nonlinear medium where, in the presence of a pair of *weak*-coupling (ω_c) and pump (ω_p) copropagating beams, Stokes and anti-Stokes photon pairs emerge (Fig. 1). The two processes, one (A) leading to the emission of a *Stokes* (ω_s) and an *anti-Stokes* (ω_{as}) photon pair and the other (B) leading to the emission of the same Stokes (ω_s) yet a different anti-Stokes ($\omega_{as'}$) photon, are sketched in Fig. 1 (red and blue lines) and governed by the following energy conservation laws $\omega_s + \omega_{as} = \omega_p + \omega_c$ and $\omega_s + \omega_{as'} = 2\omega_p$, respectively. The main feature of the scheme is that under suitable pump and coupling driving conditions (i) the probability that the two processes A and B occur simultaneously can be made to be

*alessandro.zavatta@ino.it

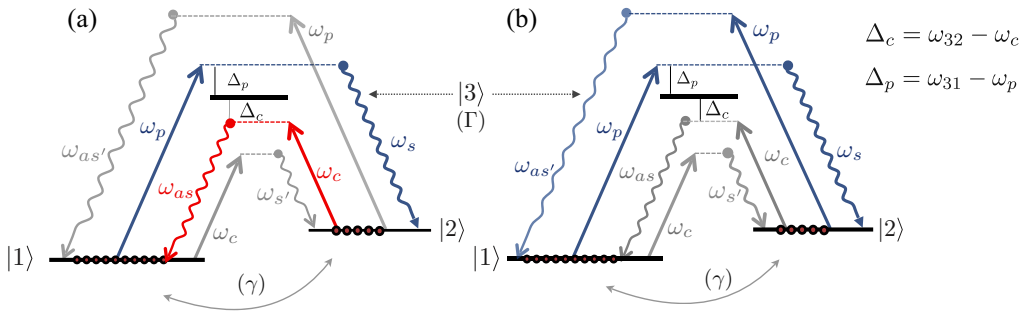

FIG. 1. Single-photon color entanglement. (a) A pair of weak-coupling (ω_c) and pump (ω_p) beams spontaneously scatter through the third-order nonlinearity of a three-level atom to generate an *anti-Stokes* photon ω_{as} (red) and a *Stokes* photon ω_s (blue). (b) Different pairs $\{\omega_{as'}, \omega_s\}$ of photons can be generated through spontaneous scattering off the pump (ω_p) alone. The spontaneous four-wave mixing processes (a) and (b) result in a small probability of generating single anti-Stokes photons at frequencies ω_{as} and $\omega_{as'}$. For certain atomic parameters ($\gamma, \Gamma, N/V$), (driving) pump and coupling detunings ($\Delta_{p,c}$) and Rabi frequencies ($\Omega_{p,c}$) (see Appendix), the emission of one single-photon through channels (a) and (b) can be made to be *undistinguishable* subject to a state-projection measurement on the Stokes (ω_s) photon (Fig. 2). The atomic levels correspond to the transition $5\,^2S_{1/2} \to 5\,^2P_{1/2}$ (^{85}Rb D_1 line) with $\lambda_{31} = 795$ nm, $\omega_{21} = 2\pi \times 3$ GHz, and decay rates $\Gamma = 2\pi \times 5.75$ MHz and $\gamma = 2\pi \times 10$ kHz.

negligible while (ii) the generation of anti-Stokes photons either through process A or through process B can be made to occur with the same probability. Hence the detection of a single Stokes photon at frequency ω_s will entail, via a state-projection measurement (Fig. 2), the emission of an anti-Stokes photon, though its detection does not reveal, even in principle, at which frequency, i.e., ω_{as} or $\omega_{as'}$, it has been emitted. Such an indistinguishability results in the state *superposition*,

$$\alpha|1\rangle_{\omega_{as}}|0\rangle_{\omega_{as'}} + \beta|0\rangle_{\omega_{as}}|1\rangle_{\omega_{as'}}. \tag{1}$$

It turns out that α and β essentially depend on the medium linear and nonlinear optical response, hence directly tunable through the pump and coupling driving fields. This state may be envisaged as the frequency-entanglement counterpart of the familiar single-photon path entanglement [15,16], or time-bin entanglement [17] that are used as important resources in quantum protocols to convey and process quantum information [18–21].

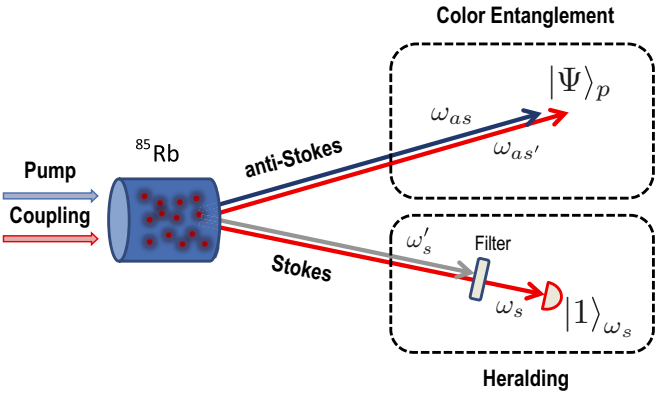

FIG. 2. Stokes state projection. Under specific pump and coupling drivings of a sample of cold ^{85}Rb atoms, pairs of pump and coupling photons scatter via spontaneous four-wave mixing into pairs of Stokes and anti-Stokes photons $\{\omega_s, \omega_{as}\}$, $\{\omega_s, \omega_{as'}\}$, $\{\omega_{s'}, \omega_{as}\}$, and $\{\omega_{s'}, \omega_{as'}\}$. A "single" photon can be shared by two different modes ω_{as} and $\omega_{as'}$ *if* a Stokes photon ω_s is detected (lower box). Such a conditional detection "heralds" the generation of the entangled state $|\Psi\rangle_p$ (upper box).

Two more processes will clearly contribute to the heralded generation of the single-photon state (1), namely, those involving the spontaneous generation of the different Stokes–anti-Stokes pairs $\{\omega_{s'}, \omega_{as'}\}$ (C) and $\{\omega_{s'}, \omega_{as}\}$ (D) also sketched in Fig. 1 (gray lines). However, the projection procedure above will prevent the processes C and D from concurring to the generation of the state (1) [22].

Entanglement generation. Assuming classical fields in the form of plane waves $E_i^+ = E_i e^{i\boldsymbol{k}_i\cdot\boldsymbol{r} - i\omega_i t}$ with $i = \{c, p\}$ respectively for the control and pump beams, and a standard field operator

$$\hat{E}_j^+ = \frac{1}{\sqrt{\pi}} \int d\omega \sqrt{\frac{2\hbar\omega}{c\epsilon_0 A}} e^{i[\boldsymbol{k}_j(\omega)\cdot\boldsymbol{r} - \omega t]} \hat{a}_j(\omega) \tag{2}$$

with $j = \{s, as\}$, for the Stokes and anti-Stokes photons propagating with a (complex) wave vector $\boldsymbol{k}_j(\omega)$ [23–25], the effective Hamiltonian describing the photon-atom interaction can be written as

$$\hat{H}_I = \frac{\epsilon_0 A}{4} \int_{-L/2}^{L/2} dz \big[\chi_A^{(3)} E_p^+ E_c^+ \hat{E}_{as}^- \hat{E}_s^- + \chi_B^{(3)} E_p^+ E_p^+ \hat{E}_{as'}^- \hat{E}_s^- + \chi_C^{(3)} E_c^+ E_p^+ \hat{E}_{as'}^- \hat{E}_{s'}^- + \chi_D^{(3)} E_c^+ E_c^+ \hat{E}_{as}^- \hat{E}_{s'}^-\big] + \text{H.c.}, \tag{3}$$

with the fields' (negative) frequency parts E_i^- and $\hat{E}_j^-$ computed as usual [23] and with space-time dependencies purposely omitted here. Here, we assume control and pump fields with a fixed relative phase relationship that can be arbitrarily controlled and tuned. The four third-order optical nonlinear susceptibilities $\chi_l^{(3)}$ for $l = \{A, B, C, D\}$ in (3) correspond to the four spontaneous nonlinear mixing processes triggered by coupling and pump. Details of the susceptibility expressions are given in the Appendix. For the sake of clarity we restrict to a nearly one-dimensional generation geometry with Stokes and anti-Stokes photons emitted in the z direction and with a fixed (transverse) mode-profile cross section A across the interaction region L. We further assume that the

Stokes and anti-Stokes modes are initially in the vacuum $|0\rangle_s|0\rangle_{s'}|0\rangle_{as}|0\rangle_{as'} \to |0\rangle$, so that in the weak spontaneous scattering limit [26], one has for the output state,

$$
\begin{aligned}
|\Psi\rangle_{\text{out}} &\simeq \left(\mathbf{1} - \frac{i}{\hbar}\int_{-\infty}^{\infty} dt\ \hat{H}_I\right)|0\rangle \\
&= |0\rangle + \int d\omega [f_A(\omega_c+\omega_p-\omega,\omega)\hat{a}^\dagger_{as}(\omega_c+\omega_p-\omega) \\
&\quad \times \hat{a}^\dagger_s(\omega) + f_B(2\omega_p-\omega,\omega)\hat{a}^\dagger_{as'}(2\omega_p-\omega)\hat{a}^\dagger_s(\omega) \\
&\quad + f_C(\omega_p+\omega_c-\omega,\omega)\hat{a}^\dagger_{as'}(\omega_p+\omega_c-\omega)\hat{a}^\dagger_{s'}(\omega) \\
&\quad + f_D(2\omega_c-\omega,\omega)\hat{a}^\dagger_{as}(2\omega_c-\omega)\hat{a}^\dagger_{s'}(\omega)] \\
&\quad \times |0\rangle_s|0\rangle_{s'}|0\rangle_{as}|0\rangle_{as'}. \qquad (4)
\end{aligned}
$$

Although states with more than one photon per frequency mode are possible (higher-order processes), they are nevertheless unlikely owing to small nonlinearities of the weak spontaneous scattering [26] we examine here, hence Eq. (4) is the generated state to a very good approximation. The four "two-photon" states are generated, in general, with *different* amplitude probabilities f_l for each of the four terms $l = \{A, B, C, D\}$ [Fig. 1(a)]. The generation of the pair $\{\omega_s, \omega_{as}\}$, e.g., occurs with the probability amplitude,

$$
f_A(\omega,\omega') = -i\frac{\sqrt{\omega\omega'}}{4\pi c}\chi_A^{(3)}(\omega,\omega')E_pE_c\,\text{sinc}\left(\frac{\Delta k_A L}{2}\right)L, \qquad (5)
$$

which depends on the electric field amplitudes (E_p, E_c) directly and through the susceptibility $\chi_A^{(3)}(\omega,\omega')$, and on the z projection $\Delta k_A = (\boldsymbol{k}_{as}+\boldsymbol{k}_s-\boldsymbol{k}_p-\boldsymbol{k}_c)\cdot\hat{\boldsymbol{z}}$ of the wave-vector mismatch (momentum conservation) for copropagating pump and coupling beams. We restrict here to collecting Stokes and anti-Stokes photon pairs that are emitted within a very small angle with respect to the z direction. Therefore, the phase mismatch is given by

$$
\begin{aligned}
\Delta k_A &= \frac{\omega_{as}}{c}n_{13}(\omega_{as}) + \frac{\omega_s}{c}n_{23}(\omega_s) \\
&\quad - \frac{\omega_p}{c}n_{13}(\omega_p) - \frac{\omega_c}{c}n_{23}(\omega_c), \qquad (6)
\end{aligned}
$$

where $n_{ij}(\omega) \approx 1 + \text{Re}[\chi_{ij}(\omega)]/2$ is the index of refraction calculated from the linear susceptibility $\chi_{ij}(\omega)$ associated with the $|i\rangle - |j\rangle$ two-level transition (see the Appendix).

The probabilities for the three other processes B, C, D are instead obtained by exchanging $c \to p$ and $as \to as'$ [to obtain $f_B(\omega,\omega')$], $c \leftrightarrow p$, $s \to s'$, and $as \to as'$ [$f_C(\omega,\omega')$], and $p \to c$ and $s \to s'$ [$f_D(\omega,\omega')$], while the same applies when computing the other mismatches $\Delta k_{B,C,D}$. It follows from (4) that the detection of a Stokes photon at frequency ω_s (Fig. 2) projects $|\Psi\rangle_{\text{out}}$ into a superposition of an anti-Stokes single photon with frequency ω_{as} and $\omega_{as'}$,

$$
\begin{aligned}
|\Psi\rangle_p &= [{}_s\langle 0|\hat{a}_s(\omega_s)]|\Psi\rangle_{\text{out}} \\
&= f_A(\omega_{as},\omega_s)|1\rangle_{as}|0\rangle_{as'} + f_B(\omega_{as'},\omega_s)|0\rangle_{as}|1\rangle_{as'}, \qquad (7)
\end{aligned}
$$

which corresponds to the state sought for in (1) with (complex) coefficients $\alpha \to f_A(\omega_{as},\omega_s)/\sqrt{\mathcal{N}}$ and $\beta \to f_B(\omega_{as'},\omega_s)/\sqrt{\mathcal{N}}$, being $\mathcal{N} = |f_A|^2 + |f_B|^2$ (normalization). Here, $|1\rangle_i = \hat{a}^\dagger(\omega_i)|0\rangle$ denotes a single-photon state at the frequency ω_i with $i = \{as, as', s, s'\}$. The degree of entanglement in $|\Psi\rangle_p$, which depends through f_A and f_B on the medium optical response (linear and nonlinear) and the wave-vector mismatch, can be all-optically controlled through pump and coupling (Fig. 1). It turns out in fact that we can span continuously from a *maximally* entangled state ($\alpha = \beta = 1/\sqrt{2}$) to a *pure* photon state [27] ($\alpha = 0$ or $\beta = 0$) directly through changing the Rabi frequencies $\Omega_{p,c}$ and detunings $\Delta_{p,c}$ [28]. We adopt here the negativity of the partial transpose (NPT) concept to quantify the degree of entanglement. This has been introduced in Ref. [29] and it is based on the Peres-Horodecki [30,31] separability criterion, thereby $NPT = 1$ corresponds to maximally entangled states and $NPT = 0$ to separable ones. For the specific state $|\Psi\rangle_p$ in (7) we have $NPT = 2|\alpha||\beta|$.

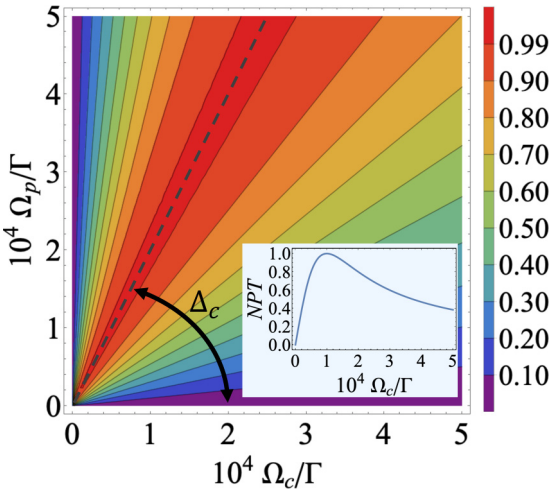

FIG. 3. Raman-like regime. Negativity of the partial transpose (NPT) for the state $|\Psi\rangle_p$ in (7) with $\Delta_p = -1$ GHz, $\Delta_c = 10$ GHz vs varying pump and coupling intensities ($\propto \Omega_{p,c}$) (see Fig. 1). For fixed driving intensities, maximum NPT values (dashed line) may be attained by tuning Δ_c. Inset: Plot of section at $\Omega_p = 2\times 10^{-4}\Gamma$; maximum entanglement is tuned through the coupling intensity ($\propto \Omega_c$). The sample has a density $N/V \simeq 5\times 10^{12}$ cm^{-3}, length $L = 100\ \mu$m.

Entanglement engineering. We will focus in the following on three representative situations to illustrate how entanglement can be efficiently engineered. We choose a realistic setup made of cold ^{85}Rb atoms [32], though we anticipate that the generation mechanism is general enough to be suited to nonatomic architectures as well [33–38].

We start by considering the case of weak driving fields and both far detuned from resonance, i.e., $\Omega_{p,c} \ll \sqrt{\gamma\Gamma}$ and $|\Delta_{p,c}| \gg \Gamma$. In these conditions, the indices of refraction for all the frequency components are very close to unity, thus phase-matching conditions are basically satisfied ($\Delta k_A, \Delta k_B \simeq 0$) over a wide range of frequencies (tens of GHz) by energy conservation. This is reported in Fig. 3 where a nearly balanced spontaneous Raman scattering regime with $NPT = 1$ over a parameter region for which $\Omega_c/\Delta_c \sim \Omega_p/\omega_{21}$ is shown. Maximum entanglement can then be directly tuned through the off-resonant coupling detuning (Δ_c) (dashed line), else through its intensity (Ω_c) (Fig. 3 inset), and can always be achieved at vanishing levels of absorption ($\mathcal{R} \sim$

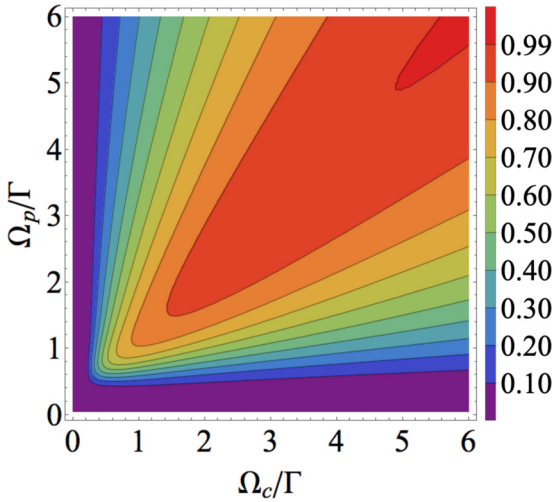

FIG. 4. Near-resonance regime. Same as in Fig. 3 with $\Delta_p = -\Gamma$, $\Delta_c = \Gamma$. The generation probability is almost constant $\mathcal{P} \sim 10^{-5}$ in the region in which $NPT > 0.9$, while it increases as NPT decreases. The anti-Stokes ω_{as} losses are constant with Ω_p yet varying with Ω_c from total absorption to $\lesssim$0.2% ($\Omega_c = 6\ \Gamma$). Anti-Stokes $\omega_{as'}$ losses, constant with Ω_c, range from a ∼3% maximum ($\Omega_p \simeq \Gamma$) to almost no loss at all ($\Omega_p = 6\Gamma$).

10^{-4}). The generation probability of the entangled state is the probability to find a single-photon state in modes ω_{as} and $\omega_{as'}$, and this is $\mathcal{P} = |\langle 1_{as}|\Psi\rangle_p|^2 + |\langle 1_{as'}|\Psi\rangle_p|^2 = |f_A|^2 + |f_B|^2$. In the spontaneous Raman regime (Fig. 3) we find values of NPT close to unity with probabilities $\mathcal{P} \sim 10^{-13}$ when background level populations are completely unbalanced ($\rho^0_{11} \gg \rho^0_{22}$).

Anti-Stokes generation probability $\mathcal{P}$ will improve *if* one or both driving fields are brought close to resonance, though absorption at each anti-Stokes mode will become crucial [24]. This turns out to be an important generation regime which we will discuss below. A proper assessment of the negativity of the partial transpose function in the presence of absorption is in order, which is done here by adopting a standard beam-splitter model [39]. According to this model, the dissipative process is formally described by means of a lossless beam splitter that mixes the ideal state with the vacuum, then the partial trace over the lossy channel returns the state subjected to losses. Thus, the lossy state appears to be noisy and attenuated by reflection of the beam splitter that accounts for absorption.

We apply this loss model to each anti-Stokes mode whose absorption $\mathcal{R}(\omega_{as,as'})$ is obtained from the imaginary part of the first-order susceptibility $\chi_{13}(\omega_{as,as'})$ (see the Appendix), i.e. $\mathcal{R}(\omega_{as,as'}) = 1 - \exp\{\mathrm{Im}[\chi_{13}(\omega_{as,as'})]\omega_{as,as'}L/c\}$. The output state affected by absorption is then used to calculate the NPT. Hereafter, a NPT close to unity will ensure the generation of a maximally entangled state with negligible absorption. We report in Fig. 4 the NPT behavior for small detunings $|\Delta_{p,c}| \sim \Gamma$ and driving fields such that $\sqrt{\gamma\Gamma} \lesssim \Omega_{p,c} \sim \Gamma$, showing large variations of the degree of entanglement along with losses and occurring with generation probabilities $\mathcal{P}$ orders of magnitudes larger than in the Raman case. Maximal entanglement ($NPT \geqslant 0.99$) is restricted only

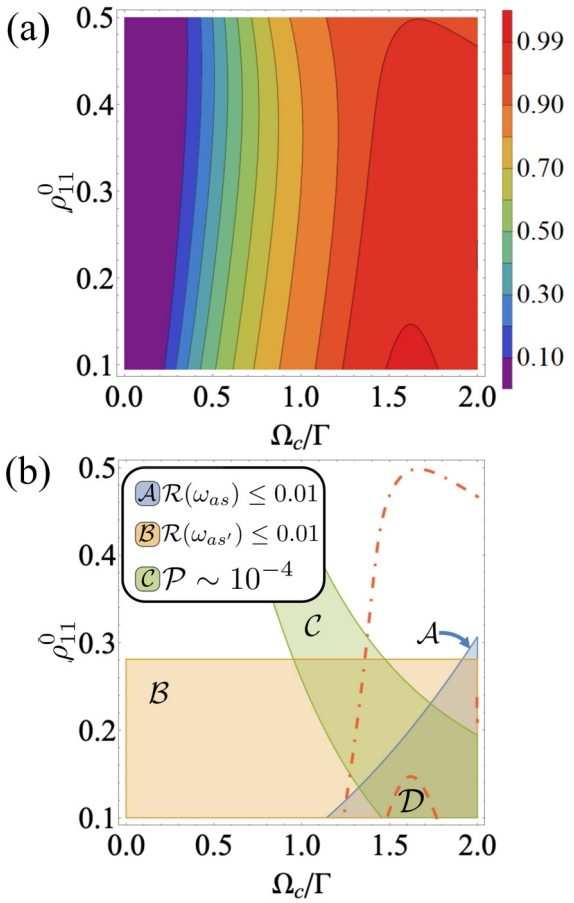

FIG. 5. Optimal entanglement. (a) Same as in Fig. 3 with $\Delta_p = -\Gamma$, $\Delta_c = \Gamma$, $\Omega_p = 1.5\Gamma$ and with varying background population values ρ^0_{11} of the lowest level [41]. (b) Contour lines for $NPT = 0.95$ (dotted dashed) and $NPT = 0.99$ (dashed) as in shown in (a). Anti-Stokes absorption $R(\omega_{as})$ decreases with Ω_c but strongly increases with ρ^0_{11} if $\Omega_c \lesssim \Gamma$. The other anti-Stokes absorption $R(\omega_{as'})$ varies in the range 0.02–0 for $0.5 > \rho^0_{11} > 0.1$ regardless of Ω_c. The overlap region ($\mathcal{D}$) between the low absorption regions ($\mathcal{A}$ and $\mathcal{B}$) yields optimal conditions to generate color entanglement ($NPT \geqslant 0.99$) with a probability $\mathcal{P} \sim 10^{-4}$ (region $\mathcal{C}$).

to the high-intensity region ($\Omega_{p,c} \sim 6\Gamma$) with probabilities $\mathcal{P} \sim 10^{-4}$ provided that $\rho^0_{11} \gg \rho^0_{22}$, i.e., most of the atomic background population (see the Appendix) is in the lowest state $|1\rangle$. Losses, on the other hand, remain small around the high-intensity region due to the Autler-Townes splitting and in the lower-intensity region due to electromagnetically induced transparency (EIT) [40].

In general, the sample optical response depends on the atom's levels steadystate background atomic populations ϱ_{jj} with $j = \{1, 2, 3\}$ (see Ref. [41]). As accurate state preparation techniques for cold ^{85}Rb samples are widely used [32], it may be worth examining how entanglement may be engineered also through state preparation.

Unlike the Raman-like regime, where the NPT behavior (Fig. 1) is unaffected by populations, changing the background population ρ^0_{11} and ρ^0_{22} of the two lower levels $|1\rangle$ and $|2\rangle$ leads instead [see Fig. 5(a)] to optimal NPT values equal or better than 0.99 at coupling strengths smaller than those of Fig. 4, with vanishing losses (<1%). A plot with all

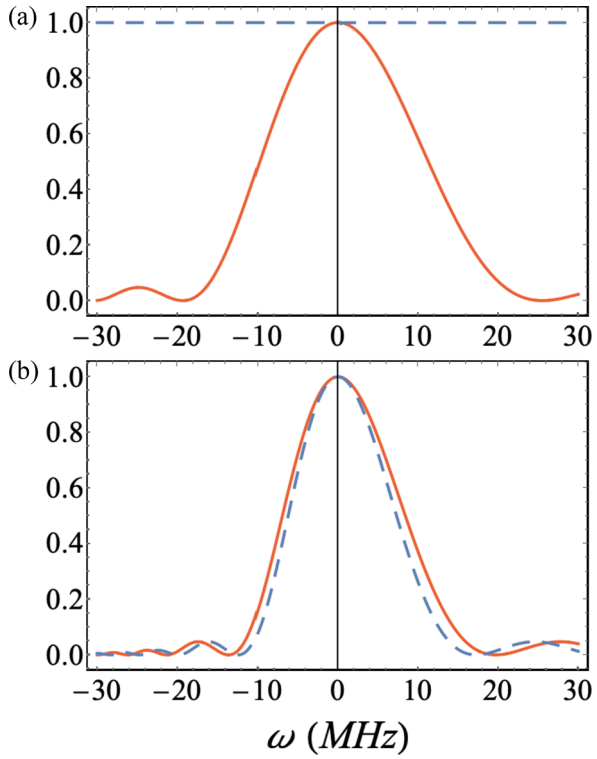

FIG. 6. Phase-matching. The plots of $\mathrm{sinc}^2(\Delta k_A L/2)$ (dashed line) and $\mathrm{sinc}^2(\Delta k_B L/2)$ (continuous line) show how the phase-matching conditions can be achieved. (a) The near-resonance parameters of Fig. 4 are used for the plots with $\Omega_p = \Omega_c = 2\Gamma$ for which the $NPT = 0.94$. (b) Optimal entanglement conditions of Fig. 5 with $\Omega_c = 1.6\Gamma$ and $\rho_{11}^0 = 0.1$ where $NPT = 0.99$.

figures of merit—NPT, $\mathcal{P}$, and absorption $\mathcal{R}$—is reported in Fig. 5(b). Optimal color entanglement is seen to take place within an overlap region for weak drivings $\Omega_{p,c} \sim |\Delta_{p,c}| \sim \Gamma$ and largely unbalanced background populations ρ_{11}^0 and ρ_{22}^0 of the two lower levels. From Fig. 5 it is clear how the manipulation of the lower populations yields to the optimization of generation as it guarantees almost the same performances in terms of NPT and $\mathcal{P}$ as those of Fig. 4 yet at much lower $\Omega_{c,p}$'s, which provides an advantage toward the implementation of the scheme with weak driving fields.

Even though NPT takes into account all the aspects connected to the state generation including phase matching through Eq. (5), it is important to show how the phase-matching conditions Δk_A and Δk_B are simultaneously satisfied in the near-resonance conditions of Figs. 4 and 5. In the former case, perfect phase matching occurs over a narrow bandwidth for the emission of ω_{as} while the $\omega_{as'}$ process is widely phase matched [as shown of Fig. 6(a)] since it occurs away from level $|3\rangle$. On the other hand, in the latter case, [as shown in Fig. 6(b)] the phase-matching conditions are satisfied simultaneously over the same range of frequencies.

In conclusion, we anticipate that the generation of heralded frequency-entangled single-photon states may occur through the Stokes state-projection scheme of Fig. 2 whereby the detection of a single-Stokes photon in the frequency mode ω_s ($\omega_{s'}$) does not reveal, even in principle, which frequency mode ω_{as} or $\omega_{as'}$ is populated by a single photon. This scenario provides a tool to develop quantum communication and information processing by exploiting the frequency degree of freedom [13]. As it is often the case for nonclassical effects of the electromagnetic field [42], the proposal for entanglement generation through the indistinguishability between two different spontaneous four-wave mixing processes exhibits a certain versatility. In principle, it could be adapted to atom photonic crystal fiber interfaces [33,34], to miniaturized (micrometer-sized) atomic vapor cells [36,43], or to solid interfaces with crystals doped with rare-earth-metal ions [37], or with with NV color centers [35,38] where similar three-level twofold configurations exist.

Acknowledgment. We are indebted to Prof. Jin Hui Wu for many insightful discussions. Support from the Italian Ministry of Foreign Affairs (MAECI) and the National Natural Science Foundation of China (NSFC) (Cooperative Program PGR05482), Ente Cassa di Risparmio di Firenze, and the Italian Ministry of University and Research (MIUR) (QSecGroundSpace) are greatly acknowledged.

APPENDIX: SUSCEPTIBILITIES

Linear susceptibilities. The atomic medium response at the anti-Stokes frequencies ω_{as} and $\omega_{as'}$ is computed through a standard density matrix approach [23,44] appropriate to the level configurations of Fig. 1. The diagonal and off-diagonal density matrix elements relevant, e.g., to the Λ configuration (red) of Fig. 1(a) are computed in the limit of a "weak" anti-Stokes field at frequency ω_{as} (nearly) two-photon resonant with a "strong" coupling (ω_c) through both lower ground levels $|1\rangle$ and $|2\rangle$. The relevant anti-Stokes susceptibility can approximately be written as,

$$\chi_{13}(\omega_{as}) = \frac{N|p_{13}|^2}{\hbar\epsilon_0}\left\{\frac{(\omega_{31}-\omega_{as}-\Delta_c-i\gamma)}{D_{as}}\varrho_{11}^0 - \frac{\alpha_c}{1+\alpha_c\frac{\Gamma_3}{\Gamma_2}}\frac{\left(\omega_{31}-\omega_{as}-i\frac{\Gamma}{2}-i\gamma\right)}{D_{as}}\varrho_{22}^0\right\}, \quad \text{(A1)}$$

where

$$D_{as} = \left(\omega_{31}-\omega_{as}-i\frac{\Gamma}{2}\right)(\omega_{31}-\omega_{as}-\Delta_c-i\gamma)-|\Omega_c|^2, \quad \text{(A2)}$$

and $\alpha_c = \frac{|\Omega_c|^2}{|\Delta_c+i\frac{\Gamma}{2}|^2}$ with $\Omega_c = \frac{\boldsymbol{p}_{32}\cdot E_c}{\hbar}$ the coupling beam Rabi frequency. We denote by E_c the electric (real) field amplitude driving the ω_{32} transition and by $\boldsymbol{p}_{32}$ the corresponding dipole moment [Fig. 1(a)]. Here, $\Delta_c = \omega_{32} - \omega_c$ denotes the *coupling*'s detuning from the resonant ω_{32} transition line while $\varrho_{11}^0 \equiv \rho_{11}^0 - \rho_{33}^0$ represents the total steady-state *background population* difference between $|1\rangle$ and $|3\rangle$ in the absence of pump and coupling and likewise for $\varrho_{22}^0 \equiv \rho_{22}^0 - \rho_{33}^0$. At thermal equilibrium the mean numbers of atoms in levels $|1\rangle$, $|2\rangle$ and $|3\rangle$ are related by the Boltzmann's law [23,32] so that one has, for instance, $N_2^0/N_1^0 \sim e^{-(E_2-E_1)/k_BT}$. In particular, $N_3^0/N_1^0 \sim N_3^0/N_2^0 \sim e^{-(E_3-E_{1,2})/k_BT} \sim 0$, a condition that is frequently matched in cold-atom experiments [32,45]. The population difference $\varrho_{jj}^0 \equiv \rho_{jj}^0 - \rho_{33}^0 \simeq \rho_{jj}^0$ amounts to the steady-state background number density $\rho_{jj}^0 = N_j^0/N$ that

one has in the absence of pump and coupling and with $N \equiv N_1^0 + N_2^0 + N_3^0 \cong N_1^0 + N_2^0$ being the total number density. Temperature, level-degeneracy, pumping, etc., are commonly used to achieve selective excitation of level $|2\rangle$ so as to vary ρ_{22}^0 [32,46–49].

The spontaneous decay rate Γ_j of level $j = \{1, 2, 3\}$ with $\Gamma_{1,2}$ much smaller than Γ_3, $\Gamma \simeq \Gamma_3$, and $\gamma \simeq (\Gamma_1 + \Gamma_2)/2$ [32]. In the absence of the coupling ($\alpha_c \to 0$), the susceptibility $\chi_{13}(\omega_{as})$ recovers the well-known expression for a two-level atom susceptibility whose real and imaginary parts yield the familiar dispersive and Lorentzian line shapes [40,50]. Likewise in the ground-state approximation [50] whereby most of the atomic background population is in the lowest state $|1\rangle$ ($\rho_{33}^0 \sim \rho_{22}^0 \sim 0$), the dominant term in (A1) recovers the well-known expression for a Λ three-level atomic susceptibility responsible for EIT [40,50,51].

The susceptibility $\chi_{13}(\omega'_{as})$ for the other anti-Stokes mode ω'_{as} can be computed using the same approach when adapted to the Λ-levels configuration (blue) of Fig. 1(b).

Nonlinear susceptibilities. The creation of photons at frequency ω_{as}, e.g., occurs through a third-order mixing process by which the *three* different weak beams $\{\omega_p, \omega_c, \omega_s\}$ interact to generate another weak beam at frequency $\omega_{as} = \omega_p + \omega_c - \omega_s$, as sketched in Fig. 1(a). The relevant third-order nonlinear susceptibility can be computed through standard perturbative expansion methods [52,53] so that under the assumption that just one (excited) energy level $|3\rangle$ contributes to intermediate resonances, the susceptibility (resonant part) comprises two terms, each proportional to the steady-state background population difference ρ_{11}^0 and ρ_{22}^0 of the two lower levels.

[1] L.-M. Duan, M. D. Lukin, J. I. Cirac, and P. Zoller, Long-distance quantum communication with atomic ensembles and linear optics, Nature (London) **414**, 413 (2001).

[2] P. Kolchin, S. Du, C. Belthangady, G. Y. Yin, and S. E. Harris, Generation of Narrow-Bandwidth Paired Photons: Use of a Single Driving Laser, Phys. Rev. Lett. **97**, 113602 (2006).

[3] B. Srivathsan, G. K. Gulati, B. Chng, G. Maslennikov, D. Matsukevich, and C. Kurtsiefer, Narrow Band Source of Transform-Limited Photon Pairs via Four-Wave Mixing in a Cold Atomic Ensemble, Phys. Rev. Lett. **111**, 123602 (2013).

[4] K. Liao, H. Yan, J. He, S. Du, Z.-M. Zhang, and S.-L. Zhu, Subnatural-Linewidth Polarization-Entangled Photon Pairs with Controllable Temporal Length, Phys. Rev. Lett. **112**, 243602 (2014).

[5] Z. Han, P. Qian, L. Zhou, J. F. Chen, and W. Zhang, Coherence time limit of the biphotons generated in a dense cold atom cloud, Sci. Rep. **5**, 9126 (2015).

[6] C. Shu, P. Chen, T. K. A. Chow, L. Zhu, Y. Xiao, M. M. T. Loy, and S. Du, Subnatural-linewidth biphotons from a Doppler-broadened hot atomic vapour cell, Nat. Commun. **7**, 12783 (2016).

[7] A. MacRae, T. Brannan, R. Achal, and A. I. Lvovsky, Tomography of a High-Purity Narrowband Photon from a Transient Atomic Collective Excitation, Phys. Rev. Lett. **109**, 033601 (2012).

[8] E. Arimondo, Laser phase spectroscopy in closed-loop multilevel schemes, Appl. Phys. B **122**, 293 (2016).

[9] A. Raczyński, J. Zaremba, and S. Zielińska-Kaniasty, Electromagnetically induced transparency and storing of a pair of pulses of light, Phys. Rev. A **69**, 043801 (2004).

[10] A. Raczyński, J. Zaremba, and S. Zielińska-Raczyńska, Pulse propagation in a medium optically dressed by three fields forming a triangular loop configuration, J. Opt. Soc. Am. B **32**, 1229 (2015).

[11] J. Roslund, R. M. de Araújo, S. Jiang, C. Fabre, and N. Treps, Wavelength-multiplexed quantum networks with ultrafast frequency combs, Nat. Photonics **8**, 109 (2014).

[12] S. Wengerowsky, S. K. Joshi, F. Steinlechner, H. Hübel, and R. Ursin, An entanglement-based wavelength-multiplexed quantum communication network, Nature (London) **564**, 225 (2018).

[13] A. Zavatta, M. Artoni, D. Viscor, and G. La Rocca, Manipulating frequency-bin entangled states in cold atoms, Sci. Rep. **4**, 3941 (2014).

[14] D. Viscor, V. Ahufinger, J. Mompart, A. Zavatta, G. C. La Rocca, and M. Artoni, Two-color quantum memory in double-Λ media, Phys. Rev. A **86**, 053827 (2012).

[15] O. Morin, J.-D. Bancal, M. Ho, P. Sekatski, V. D'Auria, N. Gisin, J. Laurat, and N. Sangouard, Witnessing Trustworthy Single-Photon Entanglement with Local Homodyne Measurements, Phys. Rev. Lett. **110**, 130401 (2013).

[16] F. Monteiro, V. C. Vivoli, T. Guerreiro, A. Martin, J.-D. Bancal, H. Zbinden, R. T. Thew, and N. Sangouard, Revealing Genuine Optical-Path Entanglement, Phys. Rev. Lett. **114**, 170504 (2015).

[17] A. Zavatta, M. D'Angelo, V. Parigi, and M. Bellini, Remote Preparation of Arbitrary Time-Encoded Single-Photon Ebits, Phys. Rev. Lett. **96**, 020502 (2006).

[18] E. Lombardi, F. Sciarrino, S. Popescu, and F. De Martini, Teleportation of a Vacuum–One-Photon Qubit, Phys. Rev. Lett. **88**, 070402 (2002).

[19] D. Salart, O. Landry, N. Sangouard, N. Gisin, H. Herrmann, B. Sanguinetti, C. Simon, W. Sohler, R. T. Thew, A. Thomas, and H. Zbinden, Purification of Single-Photon Entanglement, Phys. Rev. Lett. **104**, 180504 (2010).

[20] C. W. Chou, H. de Riedmatten, D. Felinto, S. V. Polyakov, S. J. van Enk, and H. J. Kimble, Measurement-induced entanglement for excitation stored in remote atomic ensembles, Nature (London) **438**, 828 (2005).

[21] K. S. Choi, H. Deng, J. Laurat, and H. J. Kimble, Mapping photonic entanglement into and out of a quantum memory.Nature (London) **452**, 67 (2008).

[22] Conversely, the detection of a single photon $\omega_{s'}$ will prevent the processes $\{A, B\}$ from concurring to the generation of $|\Psi\rangle$.

[23] R. Loudon, *The Quantum Theory of Light* (Clarendon, Oxford, UK, 2000).

[24] M. Artoni and R. Loudon, Propagation of nonclassical light through an absorbing and dispersive slab, Phys. Rev. A **59**, 2279 (1999).

[25] M. Artoni and R. Loudon, Quantum theory of optical-pulse propagation through an amplifying slab, Phys. Rev. A **57**, 622 (1998).

[26] S. Du, J. Wen, and M. H. Rubin, Narrowband biphoton generation near atomic resonance, J. Opt. Soc. Am. B **25**, C98 (2008).

[27] We easily recover the pure single-photon case [7] with $\alpha = 0$ setting $E_c = 0$.

[28] The relative phase of f_A and f_B in (7) can be controlled by adjusting the pump and coupling relative phase.

[29] J. Lee, M. S. Kim, Y. J. Park, and S. Lee, Partial teleportation of entanglement in a noisy environment, J. Mod. Opt. **47**, 2151 (2000).

[30] A. Peres, Separability Criterion for Density Matrices, Phys. Rev. Lett. **77**, 1 (1996).

[31] M. Horodecki, P. Horodecki, and R. Horodecki, Separability of mixed states: Necessary and sufficient conditions, Phys. Lett. A **223**, 1 (1996).

[32] C. Foot, *Atomic Physics*, 1st ed. (Oxford University Press, New York, 2005), Sec. 7.6.

[33] V. Venkataraman, K. Saha, P. Londero, and A. L. Gaeta, Few-Photon All-Optical Modulation in a Photonic Band-Gap Fiber, Phys. Rev. Lett. **107**, 193902 (2011).

[34] M. Bajcsy, S. Hofferberth, T. Peyronel, V. Balic, Q. Liang, A. S. Zibrov, V. Vuletic, and M. D. Lukin, Laser-cooled atoms inside a hollow-core photonic-crystal fiber, Phys. Rev. A **83**, 063830 (2011).

[35] M. W. Doherty, N. B. Manson, P. Delaney, F. Jelezko, J. Wrachtrup, and L. C. L. Hollenberg, The nitrogen-vacancy color center in diamond, Phys. Rep. **528**, 1 (2013).

[36] J.-M. Rost, Atomic vapour microcells: Tubes for quantum electronics, Nat. Photonics **4**, 74 (2010).

[37] Q.-Yi. He, Y. Xue, M. Artoni, G. C. La Rocca, J.-H. Xu, and J.-Y. Gao, Coherently induced stop-bands in resonantly absorbing and inhomogeneously broadened doped crystals, Phys. Rev. B **73**, 195124 (2006).

[38] J.-H. Wu, G. C. La Rocca, and M. Artoni, Controlled light-pulse propagation in driven color centers in diamond, Phys. Rev. B **77**, 113106 (2008).

[39] T. Kiss, U. Herzog, and U. Leonhardt, Compensation of losses in photodetection and in quantum-state measurements, Phys. Rev. A **52**, 2433 (1995).

[40] M. Scully and S. Zubairy, *Quantum Optics*, 1st ed. (Cambridge University Press, Cambridge, UK, 1997).

[41] The population difference $\varrho^0_{jj} = \rho^0_{jj} - \rho^0_{33} \simeq \rho^0_{jj}$ amounts to the steady-state background number density $\rho^0_{jj} = N^0_j/N$ that one has in the absence of pump and coupling and with $N \cong N^0_1 + N^0_2$ being the total (conserved) number density.

[42] M. Artoni and J. L. Birman, Non-classical states in solids and detection, Opt. Commun. **104**, 319 (1994).

[43] T. Baluktsian, C. Urban, T. Bublat, H. Giessen, R. Löw, and T. Pfau, Fabrication method for microscopic vapor cells for alkali atoms, Opt. Lett. **35**, 1950 (2010).

[44] E. Arimondo, Coherent population trapping in laser spectroscopy, in *Progress in Optics*, edited by E. Wolf, Vol. 35 (Elsevier, Amsterdam, 1996), pp. 257–354.

[45] S. Giorgini, L. P. Pitaevskii, and S. Stringari, Theory of ultracold atomic Fermi gases, Rev. Mod. Phys. **80**, 1215 (2008).

[46] D. G. C. Jones, *Atomic Physics*, 1st ed. (Chapman & Hall, London, 1997).

[47] L. Allen and D. G. C. Jones, *Principles of Gas Lasers*, 1st ed. (Butterworths, London, 1967).

[48] I. Bloch, Ultracold quantum gases in optical lattices, Nat. Phys. **1**, 23 (2005).

[49] I. Bloch, J. Dalibard, and S. Nascimbène, Quantum simulations with ultracold quantum gases, Nat. Phys. **8**, 267 (2012).

[50] P. W. Milonni, *Fast Light, Slow Light and Left-Handed Light*, 1st ed. (Taylor & Francis, London, 2004).

[51] S. Harris, Electromagnetically induced transparency, Phys. Today **50** (7), 36 (1997).

[52] H. Lotem, R.T. Lynch, and N. Bloembergen, Interference between raman resonances in four-wave difference mixing, Phys. Rev. A **14**, 1748 (1976).

[53] S. A. J. Druet, B. Attal, T. K. Gustafson, and J. P. Taran, Electronic resonance enhancement of coherent anti-Stokes Raman scattering, Phys. Rev. A **18**, 1529 (1978).